Locating the Few: Sparsity-Aware Waveform Design for Active Radar

Heng Hu, Mojtaba Soltanalian, *Member, IEEE,* Petre Stoica, *Fellow, IEEE,* and Xiaohua Zhu, *Member, IEEE*

***Abstract*—Owing to the inherent sparsity of the target scene, compressed sensing (CS) has been successfully employed in radar applications. It is known that the performance of target scene recovery in CS scenarios depends highly on the coherence of the sensing matrix (CSM), which is determined by the radar transmit waveform. In this paper, we propose efficient transmit waveform optimization approaches for two different structures of the radar waveform, namely, the single-pulse and the more general pulse-train scenarios. By determining identical coherence values associated with the sensing matrices of CS-based radars, the suggested methods provide a considerable reduction in the number of optimization variables. We show that, in the single-pulse scenario, fast Fourier transform (FFT) operations can be used to improve the computation speed, whereas, efficient power method-like iterations may be employed in the pulse-train scenarios. The effectiveness of the proposed algorithms is illustrated through several numerical examples.**

***Index Terms*—compressed sensing, mutual coherence, radar, sensing matrix, sparsity, waveform synthesis**

TABLE I
NOTATIONS

$\boldsymbol{x}(k)$	the k^{th} entry of the vector $\boldsymbol{x}$
$\|\boldsymbol{x}\|_n$	the l_n-norm of $\boldsymbol{x}$, defined as $\left(\sum_k \|\boldsymbol{x}(k)\|^n\right)^{\frac{1}{n}}$
$\boldsymbol{X}^*$	the complex conjugate of a matrix $\boldsymbol{X}$
$\boldsymbol{X}^T$	the transpose of a matrix $\boldsymbol{X}$
$\boldsymbol{X}^H$	the Hermitian transpose of a matrix $\boldsymbol{X}$
$\|\boldsymbol{X}\|_F$	the Frobenius norm of a matrix $\boldsymbol{X}$
$\mathrm{tr}(\boldsymbol{X})$	the trace of a matrix $\boldsymbol{X}$
$vec(\boldsymbol{X})$	the vector obtained by column-wise stacking of $\boldsymbol{X}$
$\mathrm{diag}(\boldsymbol{X})$	the column vector formed by the diagonal elements of $\boldsymbol{X}$
$\lambda_{\min}(\boldsymbol{X})$	the minimal eigenvalue of $\boldsymbol{X}$
$\arg(\boldsymbol{X})$	the phase angle (in radians) of $\boldsymbol{X}$
$\otimes$	the Kronecker product
$\odot$	the Hadamard product
$\mathbf{0}$	an all-zero vector/matrix
$\mathbf{1}$	an all-one vector/matrix
$\boldsymbol{I}$	the identity matrix
$\mathbb{C}$	the set of complex numbers

I. INTRODUCTION

Notation: We use bold lowercase letters for vectors and bold uppercase letters for matrices. Please see Table I for other notations used throughout this paper.

A primary interest in radar literature is the inverse problem of recovering the target scene from noisy measurements. For a radar working under the conventional Nyquist-Shannon sampling framework, the sampling rate is constrained to be at least twice the highest frequency component of the received signal in order to facilitate an accurate reconstruction of the target scene. However, in many cases, particularly for ultra wide band (UWB) radar, such a requirement is hardly achieved using the currently employed analog to digital converters (ADCs); not to mention the large computational burden caused by the processing of the data collected at high sampling rates.

The new framework of compressed sensing (CS) may promise a solution to such difficulties [2], [3]. To observe how, note that in practical radar applications, the target scene is typically sparse—i.e. there is usually a small number of targets that we are concerned with. In order to recover the data with lower sampling rates, CS relies on two criteria: (i) *sparsity*, which is related to the signal of interest (i.e. the target scene), and (ii) *incoherence*, which is related to the sensing modality to be designed.

In this paper, we consider a sparse modeling of target scene in which the targets are located in different delay-Doppler bins. A similar modeling was used in [5] and [6] to lay the ground for introducing the concept of compressed sensing radar (CSR). Extended CSR formulations for different applications such as MIMO radar [7], [8], synthetic aperture radar (SAR) [9], inverse synthetic aperture radar (ISAR) [10], and cognitive radar (CR) [11] have been investigated. In particular, it has been shown that, under the CSR framework, CS techniques can be successfully applied in radar systems, and can lead to lower sampling rates and higher resolution in radar systems.

As a key component in radar system design, the transmit waveform optimization for CSR has been considered recently, see e.g. [11], [13]. The main goal in CSR transmit waveform optimization is to reduce the coherence of an associated sensing matrix (to be defined shortly), which is determined by the radar transmit waveform. We note that transmit sequences ($\boldsymbol{s} \in \mathbb{C}^N$) with low peak-to-average power ratio (PAR),

$$\mathrm{PAR}(\boldsymbol{s}) \triangleq \frac{\|\boldsymbol{s}\|_\infty^2}{\frac{1}{N}\|\boldsymbol{s}\|_2^2}, \tag{1}$$

are very desirable for transmission purposes due to lower exposure of amplifiers to non-linear effects, as well as more uniform distribution of power through time [14]. The minimum PAR is achieved for unimodular sequences $\boldsymbol{s}$, i.e. with $|\boldsymbol{s}(k)| = 1$ for all k. As a result, we focus on the design of

This work was supported in part by the European Research Council (ERC), and the Swedish Research Council.

H. Hu and X. Zhu are with the School of Electronic Engineering and Optoelectronics Techniques, Nanjing University of Science and Technology, 210094, Nanjing, Jiangsu, China. M. Soltanalian is with the Department of Electrical and Computer Engineering, University of Illinois at Chicago, Chicago, IL 60607. P. Stoica is with the Dept. of Information Technology, Uppsala University, Uppsala, SE 75105, Sweden.

* Some parts of this work were presented at the 22nd European Signal Processing Conference (EUSIPCO) 2014 [1].

unimodular transmit sequences throughout the paper. The main contributions of this work can be summarized as follows:

- We begin our study with the single-pulse scenario which is in fact the signal model used in [15] and [11] for CSR waveform design. In this case, we propose an efficient cyclic algorithm in order to optimize the transmit waveform. This algorithm provides a reduction in the size of the Gram matrix associated with the sensing matrix, and relies on fast Fourier transform (FFT) operations to improve the computation speed; see also [1].
- The more general case of probing pulse-train is also considered. We show that the proposed algorithm for single-pulse cannot be directly extended to handle the pulse-train case. Thus, another waveform optimization algorithm is proposed to deal with the arising design problem. To the best of our knowledge, algorithms that can deal with CSR waveform design in the pulse-train scenario were not available prior to this work.

The rest of this paper is organized as follows. We discuss the sparsity-aware radar system formulation in Section II. Section III reviews the concept of mutual coherence, and its useful properties as an interesting candidate for optimization objective in radar waveform synthesis. The transmit waveform synthesis approach for single-pulse scenario is proposed in Section IV. Section V is devoted to waveform synthesis for the more general case of multi-pulse radar transmission. Simulation results are presented in Section VI.

II. System Modeling

Consider a radar system transmitting a train of $L \geq 1$ equally spaced pulses, with $s(t)$ as the complex envelope of the transmit signal at each pulse. Such a pulse-train signal model can be formulated as

$$x_T(t) = \sum_{l=0}^{L-1} s(t - lT_r),\ 0 \leq t \leq LT_r \tag{2}$$

where T_r is the pulse-to-pulse delay or the *pulse repetition interval* (PRI). We assume that $s(t)$ is non-zero solely in a time interval with size at most T_r. As mentioned earlier, we deal with two different scenarios:

- The case of $L = 1$ represents a single-pulse scenario—a basic radar signal model that has been considered in [15] and [11].
- The case of $L > 1$ corresponds to a pulse-train scenario. Pulse-train signals are usually employed in cases where the targets are in the midst of a large clutter, or a more accurate speed resolution is needed—see in particular, the signaling techniques applied in the pulse Doppler (PD) and moving target indication (MTI) radar [16].

We assume that the bandwidth B of $s(t)$ is considerably smaller than the carrier frequency f_c ($B \ll f_c$) used for transmission. Moreover, we assume that the target scene is composed of K non-fluctuating point targets from which the transmit signal will be back-scattered to the receiver. The k^{th} target is characterized by three parameters: the time delay $\tau_k = 2r_k/c$ (with c denoting the wave propagation speed) proportional to the distance r_k from the radar system to the target; the Doppler shift $f_k = 2v_k/\lambda$ (with λ being the wavelength of transmitted waveform) proportional to the radial velocity v_k of the target relative to the radar system; and the reflection coefficient α_k, proportional to the target's radar cross-section (RCS), dispersion attenuation and all other propagation factors. Base on the above, the received signal can be formulated as [17]

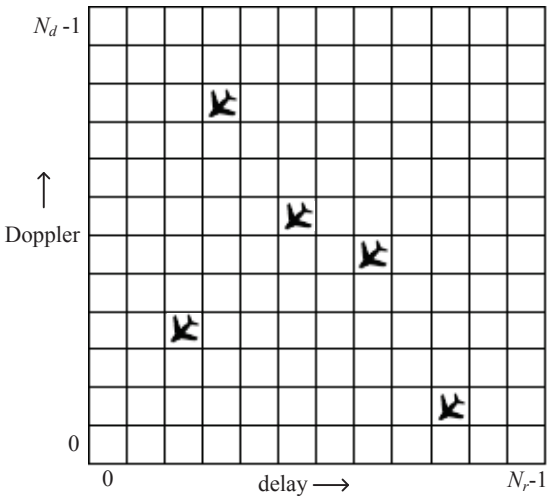

Fig. 1. The delay-Doppler plane of the target secene discretized into an $N_r \times N_d$ grid.

$$x(t) = \sum_{l=0}^{L-1} \sum_{k=1}^{K} \alpha_k s(t - \tau_k - lT_r) e^{j2\pi f_k t} + e(t) \tag{3}$$

where $e(t)$ accounts for the noise and all other unwanted interferences. Note that for an unambiguous recovery of τ_k (and equivalently, the target location information), the value of T_r must be chosen such that $T_r \geq \tau_k$, for all k.

In order to achieve an amenable formulation for sparsity-aware waveform design, in the sequel, we reformulate the received signal in a discretized framework. Specifically, we discretize the delay-Doppler plane of the target scene into an $N_r \times N_d$ grid (similar to that proposed by [15]). Fig. 1 illustrates an example of such a discretized delay-Doppler plane with $K = 5$ targets. We begin the discretization process by further noting that the received signal $x(t)$ in (3) may be rewritten by separating the parts corresponding to *fast-time* and *slow-time coding* Doppler shifts as

$$x(t) = \sum_{l=0}^{L-1} \sum_{k=1}^{K} \alpha_k s(t - \tau_k - lT_r) e^{j2\pi f_k (t - lT_r)} e^{j2\pi f_k (lT_r)} + e(t). \tag{4}$$

Define the time delay $\boldsymbol{T}^r$, the fast-time $\boldsymbol{F}_f^d$ and the slow-time $\boldsymbol{F}_s^d$ Doppler shift matrices as

$$\boldsymbol{T}^r = \begin{pmatrix} \mathbf{0}_{r\times N} \\ \boldsymbol{I}_{N\times N} \\ \mathbf{0}_{(N_r-r-1)\times N} \end{pmatrix},\ r = 0, 1, \cdots, N_r - 1, \tag{5}$$

$$\boldsymbol{F}_f^d = \begin{pmatrix} \omega_{N_d}^0 & 0 & \cdots & 0 \\ 0 & \omega_{N_d}^1 & \cdots & 0 \\ \vdots & \vdots & \ddots & \vdots \\ 0 & 0 & \cdots & \omega_{N_d}^{N-1} \end{pmatrix}^d, \quad d = 0, 1, \cdots, N_d - 1, \tag{6}$$

$$\boldsymbol{F}_s^d = \begin{pmatrix} \omega_{N_d}^{0N_p} & 0 & \cdots & 0 \\ 0 & \omega_{N_d}^{1N_p} & \cdots & 0 \\ \vdots & \vdots & \ddots & \vdots \\ 0 & 0 & \cdots & \omega_{N_d}^{(L-1)N_p} \end{pmatrix}^d, \quad d = 0, 1, \cdots, N_d - 1, \tag{7}$$

where N is the length of discretized transmit signal by uniform sampling with sampling period T_s, $\omega_{N_d} = e^{j\frac{2\pi}{N_d}}$ denotes the N_d^{th} root-of-unity, $N_p \triangleq T_r/T_s$, and (r, d) is a generic target's location in the grid. Therefore, the discrete received signal can be written as

$$\begin{aligned} \boldsymbol{x} &= \sum_{d=0}^{N_d-1} \sum_{r=0}^{N_r-1} \alpha_{r,d}\, \mathrm{diag}(\boldsymbol{F}_s^d) \otimes (\boldsymbol{T}^r \boldsymbol{F}_f^d \boldsymbol{s}) + \boldsymbol{e} \\ &= \sum_{d=0}^{N_d-1} \sum_{r=0}^{N_r-1} \alpha_{r,d}\, \boldsymbol{\varphi}_{r,d} + \boldsymbol{e} \end{aligned} \tag{8}$$

where $\boldsymbol{s}$ and $\boldsymbol{e}$ are the uniformly sampled versions of $s(t)$ and $e(t)$ with sampling period T_s, $\boldsymbol{\varphi}_{r,d} \triangleq \mathrm{diag}(\boldsymbol{F}_s^d) \otimes (\boldsymbol{T}^r \boldsymbol{F}_f^d \boldsymbol{s})$, and

$$\alpha_{r,d} = \begin{cases} \alpha_k, & \text{if the } k^{th} \text{ target is at } (r, d), \\ 0, & \text{otherwise.} \end{cases} \tag{9}$$

Interestingly, one can rewrite (8) in the matrix form as

$$\boldsymbol{x} = \boldsymbol{\Phi}\boldsymbol{\alpha} + \boldsymbol{e} \tag{10}$$

where $\boldsymbol{\Phi} = (\boldsymbol{\varphi}_{0,0}, \boldsymbol{\varphi}_{0,1}, \ldots, \boldsymbol{\varphi}_{N_r-1,N_d-1})$ and $\boldsymbol{\alpha} = (\alpha_{0,0}, \alpha_{0,1}, \ldots, \alpha_{N_r-1,N_d-1})^T$. The goal of a radar system is to estimate the location, speed, and the radar cross-section (RCS) of the targets; in other words, to find the vector $\boldsymbol{\alpha}$ in the above equation. As discussed earlier, $\boldsymbol{\alpha}$ in (10) is usually sparse. Therefore, different methods from the CS literature can be used for designing $\boldsymbol{s}$ (equivalently a low-coherence sensing matrix $\boldsymbol{\Phi}$), as well as to seek for the sparse $\boldsymbol{\alpha}$ in (10).

III. Mutual Coherence

CS techniques for handling linear formulations such as in (10) require a *low coherence* of the sensing matrix $\boldsymbol{\Phi}$ [2], [3], [18], [19]. In a set of pioneer works, it was shown that the CS-based recovery algorithms work *with high probability* if a special condition, namely the restricted isometry property (RIP) is satisfied [18]: RIP is defined with respect to an isometry constant $0 < \delta \leq 1$. For a K-sparse signal $\boldsymbol{\alpha}$ and, any non-negative integer $\sigma \leq K$, the isometry constant of $\boldsymbol{\Phi}$ is the smallest $\delta_K \geq 0$ that satisfies

$$(1 - \delta_K)\|\boldsymbol{\alpha}_\sigma\|_2^2 \leq \|\boldsymbol{\Phi}_\sigma \boldsymbol{\alpha}_\sigma\|_2^2 \leq (1 + \delta_K)\|\boldsymbol{\alpha}_\sigma\|_2^2 \tag{11}$$

where $\boldsymbol{\Phi}_\sigma$ is a subset of σ columns arbitrarily extracted from $\boldsymbol{\Phi}$, and $\boldsymbol{\alpha}_\sigma$ is the reflection coefficient vector corresponding to the σ selected columns. The RIP condition then implies that any σ subset of columns in $\boldsymbol{\Phi}$ with cardinality less than K is *nearly* orthogonal.

Due to the typically difficult nature of verifying RIP, other measures of coherence were investigated in the literature. The mutual coherence [20], also known as coherence of the sensing matrix (CSM), is an alternative framework for measuring the incoherence required by CS, which can be defined as

$$\mu(\boldsymbol{\Phi}) = \max_{(r,d) \neq (r',d')} \frac{\left| \boldsymbol{\varphi}_{r,d}^H \boldsymbol{\varphi}_{r',d'} \right|}{\|\boldsymbol{\varphi}_{r,d}\|_2 \|\boldsymbol{\varphi}_{r',d'}\|_2}. \tag{12}$$

An interesting property of mutual coherence is as follows [3]: Suppose the sparsity order of an estimated target scene $\tilde{\boldsymbol{\alpha}}$ satisfies the inequality

$$\|\tilde{\boldsymbol{\alpha}}\|_0 < \frac{1}{2}\left(1 + \frac{1}{\mu(\boldsymbol{\Phi})}\right). \tag{13}$$

Then $\tilde{\boldsymbol{\alpha}}$ is necessarily the sparsest solution of the linear equation $\boldsymbol{x} = \boldsymbol{\Phi}\boldsymbol{\alpha}$. Moreover, fast greedy algorithms such as the basis pursuit (BP) or the orthogonal matching pursuit (OMP) are guaranteed to find the correct solution $\boldsymbol{\alpha}$ [3].

A suitable approach to describe $\mu(\boldsymbol{\Phi})$ is via the Gram matrix $\boldsymbol{G} \triangleq \tilde{\boldsymbol{\Phi}}^H \tilde{\boldsymbol{\Phi}}$, where $\tilde{\boldsymbol{\Phi}}$ is the column-normalized version of $\boldsymbol{\Phi}$. Consequently, $\mu(\boldsymbol{\Phi})$ can be stated as

$$\mu(\boldsymbol{\Phi}) = \max_{k \neq l} |\boldsymbol{G}(k, l)| \tag{14}$$

where $\{|\boldsymbol{G}(k,l)|\}_{k \neq l}$ are the *coherence coefficients* associated with the sensing matrix $\boldsymbol{\Phi}$.[1] Note that a matrix $\boldsymbol{\Phi}$ with low coherence corresponds to a Gram matrix $\boldsymbol{G}$ which is close to identity $\boldsymbol{I}$. As a result, one can effectively reduce $\mu(\boldsymbol{\Phi})$ by solving the optimization problem:

$$\min_{\boldsymbol{\Phi}} \ \|\boldsymbol{G} - \boldsymbol{I}\|_F^2 \tag{15}$$

Although (15) might be easier to tackle compared to a direct minimization of $\mu(\boldsymbol{\Phi})$, a large number of variables can still make the problem prohibitive. In the following sections, we will discuss more effective approaches that formulate a quadratic alternative of (15), and particularly in the scenario of single-pulse, we show that FFT operations can be used to improve the computation speed.

IV. Single-pulse (Corresponding to $L = 1$)

In this section, we devise an efficient algorithm for transmit sequence design in the single-pulse case. Note that when the number of pulses is limited to one, we have $\boldsymbol{F}_s = 1$, and thus, the Doppler shifts are only due to the fast-time component $\boldsymbol{F}_f = \boldsymbol{F}$. In particular, the coherence between any two arbitrary columns of the matrix $\tilde{\boldsymbol{\Phi}}$ (or equivalently the corresponding element in the Gram matrix $\boldsymbol{G}$) can be written

[1] We note that, according to the formulation in (8), the coherence coefficients can also be associated with the transmit sequence $\boldsymbol{s}$.

as

$$\begin{aligned}\tilde{\boldsymbol{\varphi}}_{r,d}^{H}\tilde{\boldsymbol{\varphi}}_{r',d'} &= \left(\frac{1}{\sqrt{N}}\boldsymbol{T}^{r}\boldsymbol{F}^{d}\boldsymbol{s}\right)^{H}\left(\frac{1}{\sqrt{N}}\boldsymbol{T}^{r'}\boldsymbol{F}^{d'}\boldsymbol{s}\right)\\ &= \frac{1}{N}\left(\boldsymbol{s}^{H}\left(\boldsymbol{F}^{d}\right)^{H}\boldsymbol{T}^{r\,H}\right)\left(\boldsymbol{T}^{r'}\boldsymbol{F}^{d'}\boldsymbol{s}\right)\\ &= \frac{1}{N}\boldsymbol{s}^{H}\left(\boldsymbol{F}^{d}\right)^{H}\widetilde{\boldsymbol{T}}_{\Delta r}\boldsymbol{F}^{d'}\boldsymbol{s} \end{aligned} \tag{16}$$

where $\widetilde{\boldsymbol{T}}_{\Delta r} = \boldsymbol{T}^{r\,H}\boldsymbol{T}^{r'}$ is a square shifting matrix[2] of size $N\times N$, and $\Delta r = r'-r$. Using (16), the optimization problem (15) can be equivalently written as

$$\begin{aligned}\min_{\boldsymbol{s}} \quad & \eta \\ \text{s.t.} \quad & |\boldsymbol{s}_n| = 1,\ n = 1,\dots,N.\end{aligned} \tag{17}$$

where

$$\begin{aligned}\eta &= \left\| \begin{pmatrix} \widetilde{\boldsymbol{G}}_0 & \widetilde{\boldsymbol{G}}_1 & \cdots & \widetilde{\boldsymbol{G}}_{N_r-1} \\ \widetilde{\boldsymbol{G}}_{-1} & \widetilde{\boldsymbol{G}}_0 & \cdots & \widetilde{\boldsymbol{G}}_{N_r-2} \\ \vdots & \vdots & \ddots & \vdots \\ \widetilde{\boldsymbol{G}}_{1-N_r} & \widetilde{\boldsymbol{G}}_{2-N_r} & \cdots & \widetilde{\boldsymbol{G}}_0 \end{pmatrix} - \boldsymbol{I} \right\|_F^2 \\ &= N_r \left\|\widetilde{\boldsymbol{G}}_0 - \boldsymbol{I}\right\|_F^2 + \sum_{0<|r|\le N-1} (N_r - |r|)\left\|\widetilde{\boldsymbol{G}}_r\right\|_F^2 \\ &= \sum_{r=-(N-1)}^{N-1} \gamma_r^2 \left\|\widetilde{\boldsymbol{G}}_r - \boldsymbol{I}\delta_r\right\|_F^2 \end{aligned} \tag{18}$$

and

$$\widetilde{\boldsymbol{G}}_r = \boldsymbol{X}^H \widetilde{\boldsymbol{T}}_r \boldsymbol{X}, \tag{19}$$

$$\boldsymbol{X} = (\boldsymbol{x}_0, \boldsymbol{x}_1, \dots, \boldsymbol{x}_{N_d-1}), \tag{20}$$

$$\boldsymbol{x}_d = \frac{1}{\sqrt{N}}\boldsymbol{F}^d\boldsymbol{s} \quad , \quad d = 0,1,\dots,N_d-1, \tag{21}$$

$$\gamma_r^2 = \begin{cases} N_r - |r|, & |r| < N_r, \\ 0, & \text{otherwise}, \end{cases} \tag{22}$$

and δ_r denotes the Kronecker delta function:

$$\delta_r = \begin{cases} 1, & r = 0, \\ 0, & r \neq 0. \end{cases} \tag{23}$$

It is worth observing that, the summation in (18) paves the way for a significant reduction in the dimension of the employed matrix variables.

Next note that $\widetilde{\boldsymbol{T}}_r$ is a shifting matrix, and hence $\widetilde{\boldsymbol{G}}_r$ can be viewed as the covariance matrix of the vectors $\{\boldsymbol{x}_d\}$ corresponding to the time lag r. Based on this observation, the following Parseval-type equality holds [21]:

$$\begin{aligned}\|\boldsymbol{G} - \boldsymbol{I}\|_F^2 &= \sum_{r=-(N-1)}^{N-1} \gamma_r^2 \left\|\widetilde{\boldsymbol{G}}_r - \boldsymbol{I}\delta_r\right\|_F^2 \\ &= \frac{1}{2N}\sum_{p=1}^{2N}\left\|\boldsymbol{\Psi}\left(\frac{2\pi p}{2N}\right) - \gamma_0\boldsymbol{I}\right\|_F^2 \end{aligned} \tag{24}$$

[2]Note that, in contrast to $\{\boldsymbol{T}^r\}$, the shifting matrices $\left\{\widetilde{\boldsymbol{T}}_{\Delta r}\right\}$ perform the shift operation in an N-length time frame, which implies that some parts of the signal may be dropped.

in which

$$\boldsymbol{\Psi}(\omega) = \sum_{r=-(N-1)}^{N-1} \gamma_r \boldsymbol{X}^H \widetilde{\boldsymbol{T}}_r \boldsymbol{X}\, e^{-j\omega r} \tag{25}$$

represents the spectral density matrix of the (vector) sequence $[\boldsymbol{x}_0(r), \boldsymbol{x}_1(r), \dots, \boldsymbol{x}_{N_d-1}(r)]^T$.

Interestingly, the frequency domain criterion in (24) has the same form as (28) in [21]. Therefore, we employ a similar approach to tackle the problem herein. In particular, the $\boldsymbol{\Psi}(\omega)$ defined in (25) can also be written in the form

$$\boldsymbol{\Psi}(\omega) = \boldsymbol{Z}^H(\omega)\boldsymbol{\Gamma}\boldsymbol{Z}(\omega) \tag{26}$$

with

$$\boldsymbol{Z}(\omega) = (\boldsymbol{z}(1)e^{-j\omega}, \dots, \boldsymbol{z}(N)e^{-j\omega N})^T, \tag{27}$$

$$\boldsymbol{z}(n) = (\boldsymbol{x}_0(n), \dots, \boldsymbol{x}_{N_d-1}(n))^T \tag{28}$$

for $1 \le n \le N$, and

$$\boldsymbol{\Gamma} = \begin{pmatrix} \gamma_0 & \gamma_1 & \cdots & \gamma_{N-1} \\ \gamma_{-1} & \gamma_0 & \cdots & \vdots \\ \vdots & \vdots & \ddots & \gamma_1 \\ \gamma_{-N+1} & \cdots & \gamma_{-1} & \gamma_0 \end{pmatrix}. \tag{29}$$

As a result, we have that

$$\|\boldsymbol{G} - \boldsymbol{I}\|_F^2 = \frac{1}{2N}\sum_{p=1}^{2N}\left\|\boldsymbol{Z}_p^H\boldsymbol{\Gamma}\boldsymbol{Z}_p - \gamma_0\boldsymbol{I}\right\|_F^2 \tag{30}$$

where $\boldsymbol{Z}_p \triangleq \boldsymbol{Z}(2\pi p/(2N))$. Note that (30) is *quartic* with respect to $\boldsymbol{s}$. Observe that $\left\|\widetilde{\boldsymbol{G}}_0 - \boldsymbol{I}\right\|_F^2$ is constant, and thus, a diagonal loading of $\boldsymbol{\Gamma}$ does not change the solution to (15). Let $\tilde{\gamma_0} = \gamma_0 + \lambda$ and $\tilde{\boldsymbol{\Gamma}} = \boldsymbol{\Gamma} + \lambda\boldsymbol{I}$, with λ being a non-negative scalar that ensures $\tilde{\boldsymbol{\Gamma}} \succeq 0$. Moreover, let $\boldsymbol{C}$ represent the Hermitian square root of $\tilde{\boldsymbol{\Gamma}}$, i.e. $\boldsymbol{C}^H\boldsymbol{C} = \tilde{\boldsymbol{\Gamma}}$. An instrumental observation from the equivalence properties of Hermitian square roots is that $\boldsymbol{Z}_p^H\tilde{\boldsymbol{\Gamma}}\boldsymbol{Z}_p$ is *close* to scaled identity $\tilde{\gamma_0}\boldsymbol{I}$, if and only if there exists a unitary matrix $\boldsymbol{U}_p$ for which $\boldsymbol{C}\boldsymbol{Z}_p$ is *close* to $\sqrt{\tilde{\gamma_0}}\boldsymbol{U}_p$; in particular, one pair of the latter quantities achieves equality if and only if an equality is attained for its counterpart. Consequently, one can reduce the coherence of $\boldsymbol{\Phi}$ conveniently using the following *quadratic* alternative of (30):

$$\begin{aligned}\min_{\boldsymbol{s},\boldsymbol{U}_p} \quad & \sum_{p=1}^{2N}\left\|\boldsymbol{C}\boldsymbol{Z}_p - \sqrt{\tilde{\gamma_0}}\boldsymbol{U}_p\right\|_F^2 \\ \text{s.t.} \quad & |\boldsymbol{s}_n| = 1, \qquad n = 1,\dots,N, \\ & \boldsymbol{U}_p^H\boldsymbol{U}_p = \boldsymbol{I},\ p = 1,\dots,2N. \end{aligned} \tag{31}$$

To tackle the minimization problem in (31), we adopt a cyclic method as follows. For given $\{\boldsymbol{Z}_p\}_{p=1}^{2N}$ (equivalently a given transmit sequence $\boldsymbol{s}$), let

$$\boldsymbol{Z}_p^H\boldsymbol{C}^H = \boldsymbol{U}_{p,1}\boldsymbol{\Sigma}\boldsymbol{U}_{p,2}^H \tag{32}$$

represent the *economy-size* singular value decomposition (SVD) of $\boldsymbol{Z}_p^H\boldsymbol{C}^H$, with $\boldsymbol{U}_{p,1}$ being an $N_d\times N_d$ unitary matrix, $\boldsymbol{\Sigma}$ being an $N_d \times N_d$ diagonal matrix, and $\boldsymbol{U}_{p,2}$ being an

$N \times N_d$ semi-unitary matrix. Then the minimizer $\boldsymbol{U}_p$ of (31) is given by [21]

$$\boldsymbol{U}_p = \boldsymbol{U}_{p,2}\, \boldsymbol{U}_{p,1}^H. \tag{33}$$

Similar to the WeCAN algorithm in [21], the computation of $\boldsymbol{C}\boldsymbol{Z}_p$ can be performed using the FFT operations. To observe how, let

$$\tilde{\boldsymbol{X}}_m = \boldsymbol{C}^T \odot (\boldsymbol{x}_m, \boldsymbol{x}_m, \ldots, \boldsymbol{x}_m)_{N\times N} \tag{34}$$

for $0 \le m \le N_d - 1$, and

$$\hat{\boldsymbol{F}} = \sqrt{2N}\boldsymbol{A}^H \tilde{\boldsymbol{F}}, \tag{35}$$

$$\tilde{\boldsymbol{F}} = \begin{pmatrix} \tilde{\boldsymbol{X}}_0 & \ldots & \tilde{\boldsymbol{X}}_{N_d-1} \\ \boldsymbol{0}_{N\times N} & \ldots & \boldsymbol{0}_{N\times N} \end{pmatrix} \tag{36}$$

where $\boldsymbol{A}$ denotes the $2N \times 2N$ (inverse) DFT matrix, whose (l,p)-element is given by

$$[A]_{l,p} = \frac{1}{\sqrt{2N}}\, e^{j2\pi lp/(2N)}, \quad l,p = 1,\ldots,2N. \tag{37}$$

Using the above formulations, one can observe that the $N\times N_d$ matrix $\boldsymbol{C}\boldsymbol{Z}_p$ may be obtained by reshaping the $NN_d\times 1$ vector $\boldsymbol{f}_p$ into each column of $\boldsymbol{C}\boldsymbol{Z}_p$, where $\boldsymbol{f}_p^T$ represents the p^{th} row of $\hat{\boldsymbol{F}}$.

Next we discuss the minimization of (31) with respect to $\boldsymbol{s}$ for given $\{\boldsymbol{U}_p\}_{p=1}^{2N}$. Let

$$\boldsymbol{V}_{2N\times NN_d} = (\boldsymbol{v}_1, \boldsymbol{v}_2, \ldots, \boldsymbol{v}_{2N})^T \tag{38}$$

where $\boldsymbol{v}_p = \sqrt{\gamma_0}\; vec(\boldsymbol{U}_p)$, $1 \le p \le 2N$. Then the criterion in (31) can be written as

$$\begin{aligned}\sum_{p=1}^{2N} \|\boldsymbol{C}\boldsymbol{Z}_p - \sqrt{\gamma_0}\boldsymbol{U}_p\|_F^2 &= \left\|\sqrt{2N}\boldsymbol{A}^H\tilde{\boldsymbol{F}} - \boldsymbol{V}\right\|_F^2 \\ &= 2N\left\|\tilde{\boldsymbol{F}} - \frac{1}{\sqrt{2N}}\boldsymbol{A}\boldsymbol{V}\right\|_F^2. \end{aligned} \tag{39}$$

Note that (39) can be minimized with respect to each element of $\boldsymbol{s}$ in a separate manner. Particularly, we can consider minimizing the following criterion with respect to s (i.e. a generic element of $\boldsymbol{s}$):

$$\sum_{k=1}^{NN_d} |\mu_k s - \nu_k|^2 = H - 2\,\Re\left[\left(\sum_{k=1}^{NN_d}\mu_k^*\nu_k\right)s^*\right] \tag{40}$$

where $\{\mu_k\}$ are given by the elements of $\tilde{\boldsymbol{F}}$ that contain s, ν_k is given by the element of $\frac{1}{\sqrt{2N}}\boldsymbol{A}\boldsymbol{V}$ whose position is the same as that of μ_k in $\tilde{\boldsymbol{F}}$, and

$$\begin{aligned} H &= \sum_{k=1}^{NN_d}|\mu_k s|^2 + \sum_{k=1}^{NN_d}|\nu_k|^2 \\ &= \sum_{k=1}^{NN_d}|\mu_k|^2 + \sum_{k=1}^{NN_d}|\nu_k|^2 \end{aligned} \tag{41}$$

is a constant. Therefore, the unimodular s minimizing (40) can be obtained as

$$\begin{aligned} s &= e^{j\varphi}, \\ \varphi &= \arg\left(\sum_{k=1}^{NN_d}\mu_k^*\nu_k\right). \end{aligned} \tag{42}$$

TABLE II
THE ALGORITHM FOR SPARSITY-AWARE TRANSMIT SEQUENCE DESIGN (SINGLE-PULSE CASE)

Step 0: Initialize the transmit sequence $\boldsymbol{s}$ with a random unimodular sequence (or by a good existing sequence). Calculate the Hermitian square root $\boldsymbol{C}$ of $\tilde{\boldsymbol{\Gamma}}$.
Step 1: Fix $\boldsymbol{s}$ (equivalently $\{\boldsymbol{Z}_p\}_{p=1}^{2N}$) and compute $\{\boldsymbol{U}_p\}_{p=1}^{2N}$ using (33).
Step 2: Fix $\{\boldsymbol{U}_p\}_{p=1}^{2N}$ and compute $\boldsymbol{s}$ using (42).
Step 3: Repeat steps 1 and 2 until a stop criterion is satisfied, e.g. $\|\boldsymbol{s}^{(t+1)} - \boldsymbol{s}^{(t)}\|_F < \varepsilon$ for some given $\varepsilon > 0$, where t denotes the total iteration number.

Finally, the steps of the proposed algorithm for designing the transmit sequence $\boldsymbol{s}$ are summarized in Table II. From a complexity viewpoint, the suggested algorithm relies on a one-time computation of $\boldsymbol{C}$ with an $\mathcal{O}(N^3)$ cost. At each iteration, the proposed method requires $2NN_d$ computation of $2N$-point (I)FFTs, as well as $2N$ computations of the SVD of an $N_d \times N$ matrix. Owing to efficient FFT operations, the method appears to be considerably less expensive than the matrix-based method in [11] as the transmit sequence length N grows large—see [1] for a numerical comparison.

V. PULSE-TRAIN (CORRESPONDING TO $L > 1$)

In this section, we will consider the design of radar transmit waveform in pulse-train scenario with $L > 1$. One can easily observe that if $L > 1$, the slow-time Doppler shift matrix $\boldsymbol{F}_s^d$ is no longer identical/constant for different Doppler shifts d. Thus, the simplifying formulations associated with single-pulse scenario cannot be directly extended to the pulse-train case. Additionally, we note that although the pulse-train formulation below is also valid for $L = 1$, it does not present a similar potential for using FFT operations—instead, we achieve a general framework based on unimodular quadratic programs (UQPs) and resort to a fast approach to handle such optimization problems.

To begin describing the design methodology, we note that the coherence between any two arbitrary columns of the matrix $\tilde{\boldsymbol{\Phi}}$ (and equivalently the corresponding element in the Gram matrix $\boldsymbol{G}$) can be written as

$$\begin{aligned} \tilde{\boldsymbol{\varphi}}_{r,d}^H\tilde{\boldsymbol{\varphi}}_{r',d'} &= \left[\frac{1}{\sqrt{LN}}\mathrm{diag}(\boldsymbol{F}_s^d)\otimes(\boldsymbol{T}^r\boldsymbol{F}_f^d\boldsymbol{s})\right]^H \\ &\quad\times\left[\frac{1}{\sqrt{LN}}\mathrm{diag}(\boldsymbol{F}_s^{d'})\otimes(\boldsymbol{T}^{r'}\boldsymbol{F}_f^{d'}\boldsymbol{s})\right] \\ &= \frac{1}{LN}\left[\left(\mathrm{diag}(\boldsymbol{F}_s^d)\right)^H\otimes\left(\boldsymbol{s}^H\left(\boldsymbol{F}_f^d\right)^H(\boldsymbol{T}^r)^H\right)\right] \\ &\quad\times\left[\mathrm{diag}(\boldsymbol{F}_s^{d'})\otimes(\boldsymbol{T}^{r'}\boldsymbol{F}_f^{d'}\boldsymbol{s})\right] \\ &= \frac{1}{LN}\,\mathrm{tr}\left(\boldsymbol{F}_s^{\Delta d}\right)\left[\boldsymbol{s}^H\left(\boldsymbol{F}_f^d\right)^H\boldsymbol{T}^{\Delta r}\boldsymbol{F}_f^{d'}\boldsymbol{s}\right] \\ &= \frac{1}{LN}\sum_{l=0}^{L-1}\sum_{n=N_l}^{N_u}s_n^*s_{n-\Delta r}e^{j\frac{2\pi}{M}(N_pl+n)\Delta d} \\ &\quad\times e^{-j\frac{2\pi}{M}\Delta r d'} \end{aligned} \tag{43}$$

where $\widetilde{\boldsymbol{T}}_{\Delta r} = \boldsymbol{T}^{rH}\boldsymbol{T}^{r'}$, $\Delta r = r' - r$, $\Delta d = d' - d$, $N_l = \max\{1, 1+\Delta r\}$ and $N_u = \min\{N, N+\Delta r\}$. Based on the

above equation, it is easy to verify that the absolute values of $\tilde{\boldsymbol{\varphi}}_{r,d}^H \tilde{\boldsymbol{\varphi}}_{r',d'}$, with the same Δr and Δd are all identical. As a result, the Gram matrix $\boldsymbol{G}$ has a specific structure that can be exploited; specifically, with a change of variables, one can write an element of $\boldsymbol{G}$ (associated with a range shift index r and Doppler shift index d) as

$$\begin{aligned} g(r,d) &= \frac{1}{LN} \sum_{l=0}^{L-1} \sum_{n=N_l}^{N_u} s_n^* s_{n-r} e^{j\frac{2\pi}{M}(N_p l+n)d} \\ &= \frac{1}{LN} \operatorname{tr}\left(\boldsymbol{F}_s^d\right) \left(\boldsymbol{s}^H \left(\boldsymbol{F}_f^d\right)^H \widetilde{\boldsymbol{T}}_r \boldsymbol{s}\right) \\ &= \boldsymbol{s}^H \boldsymbol{Q}_{r,d} \boldsymbol{s} \end{aligned} \tag{44}$$

where

$$\boldsymbol{Q}_{r,d} = \left(\operatorname{tr}\left(\boldsymbol{F}_s^d\right)/LN\right) \left(\boldsymbol{F}_f^d\right)^H \widetilde{\boldsymbol{T}}_r. \tag{45}$$

Therefore, by using (43) and (44), we can consider the following optimization problem instead of (15) for coherence reduction:

$$\begin{aligned} \min_{\boldsymbol{s}} \quad & \zeta \\ \text{s.t.} \quad & |\boldsymbol{s}_n| = 1, n = 1, \ldots, N. \end{aligned} \tag{46}$$

where

$$\begin{aligned} \zeta &= \sum_{r=0}^{N_r-1} \sum_{\substack{d=-(N_d-1) \\ (r,d)\neq(0,0)}}^{N_d-1} |g(r,d)|^2 \\ &= \sum_{r=0}^{N_r-1} \sum_{\substack{d=-(N_d-1) \\ (r,d)\neq(0,0)}}^{N_d-1} |\boldsymbol{s}^H \boldsymbol{Q}_{r,d} \boldsymbol{s}|^2 \end{aligned} \tag{47}$$

and $g(-r,d) = g^*(r,-d)$ due to (44). It is worthwhile to make a remark similar to the single-pulse case herein, i.e., in light of the observation below (43), (46) leads to a significant reduction in the number of coherence terms one should try to make smaller via the waveform design.

To tackle the optimization problem proposed in (46), we first let

$$\widetilde{\boldsymbol{Q}}_{r,d} = \frac{1}{2}\left(\boldsymbol{Q}_{r,d} + \boldsymbol{Q}_{r,d}^H\right) \tag{48}$$

$$\widehat{\boldsymbol{Q}}_{r,d} = \frac{1}{2}\left(\boldsymbol{Q}_{r,d} - \boldsymbol{Q}_{r,d}^H\right) \tag{49}$$

where $\widetilde{\boldsymbol{Q}}_{r,d}$ and $\widehat{\boldsymbol{Q}}_{r,d}$ are Hermitian and skew-Hermitian matrices respectively. The latter transformation of variables ensures that

$$\begin{cases} \boldsymbol{s}^H \widetilde{\boldsymbol{Q}}_{r,d} \boldsymbol{s} & \rightarrow \text{ is real-valued,} \\ \boldsymbol{s}^H \widehat{\boldsymbol{Q}}_{r,d} \boldsymbol{s} & \rightarrow \text{ is imaginary.} \end{cases} \tag{50}$$

It follows from (50) that

$$\begin{aligned} \left|\boldsymbol{s}^H \boldsymbol{Q}_{r,d} \boldsymbol{s}\right|^2 &= \left|\boldsymbol{s}^H (\widetilde{\boldsymbol{Q}}_{r,d} + \widehat{\boldsymbol{Q}}_{r,d}) \boldsymbol{s}\right|^2 \\ &= \left|\boldsymbol{s}^H \widetilde{\boldsymbol{Q}}_{r,d} \boldsymbol{s}\right|^2 + \left|\boldsymbol{s}^H \widehat{\boldsymbol{Q}}_{r,d} \boldsymbol{s}\right|^2 \\ &= \left|\boldsymbol{s}^H \widetilde{\boldsymbol{Q}}_{r,d} \boldsymbol{s}\right|^2 + \left|\boldsymbol{s}^H j\widehat{\boldsymbol{Q}}_{r,d} \boldsymbol{s}\right|^2 \end{aligned} \tag{51}$$

where $j = \sqrt{-1}$ and $j\widehat{\boldsymbol{Q}}_{r,d}$ is a Hermitian matrix. It follows from (51) that the objective function ζ can be rewritten as

$$\begin{aligned} \zeta &= \sum_{r=0}^{N_r-1} \sum_{\substack{d=-(N_d-1) \\ (r,d)\neq(0,0)}}^{N_d-1} \left\{ \left|\boldsymbol{s}^H \widetilde{\boldsymbol{Q}}_{r,d} \boldsymbol{s}\right|^2 + \left|\boldsymbol{s}^H j\widehat{\boldsymbol{Q}}_{r,d} \boldsymbol{s}\right|^2 \right\} \\ &= \sum_{r=0}^{N_r-1} \sum_{\substack{d=-(N_d-1) \\ (r,d)\neq(0,0)}}^{N_d-1} \left\{ \left|\boldsymbol{s}^H (\widetilde{\boldsymbol{Q}}_{r,d} + \lambda \boldsymbol{I}) \boldsymbol{s} - \lambda N\right|^2 \right. \\ &\qquad \left. + \left|\boldsymbol{s}^H (j\widehat{\boldsymbol{Q}}_{r,d} + \lambda \boldsymbol{I}) \boldsymbol{s} - \lambda N\right|^2 \right\} \\ &= \sum_{r=0}^{N_r-1} \sum_{\substack{d=-(N_d-1) \\ (r,d)\neq(0,0)}}^{N_d-1} \left\{ \left|\boldsymbol{s}^H \widetilde{\boldsymbol{Q}'}_{r,d} \boldsymbol{s} - \lambda N\right|^2 \right. \\ &\qquad \left. + \left|\boldsymbol{s}^H \widehat{\boldsymbol{Q}'}_{r,d} \boldsymbol{s} - \lambda N\right|^2 \right\} \end{aligned} \tag{52}$$

where $\widetilde{\boldsymbol{Q}'}_{r,d} = \widetilde{\boldsymbol{Q}}_{r,d} + \lambda \boldsymbol{I}$, $\widehat{\boldsymbol{Q}'}_{r,d} = j\widehat{\boldsymbol{Q}}_{r,d} + \lambda \boldsymbol{I}$, and where $\lambda \in \mathbb{R}$ is chosen such that

$$\lambda > -\min\left(\bigcup_{r,d} \left\{\lambda_{\min}\left(\widetilde{\boldsymbol{Q}'}_{r,d}\right), \lambda_{\min}\left(\widehat{\boldsymbol{Q}'}_{r,d}\right)\right\}\right) \tag{53}$$

to ensure the positive-definiteness of $\left\{\widetilde{\boldsymbol{Q}'}_{r,d}\right\}$ and $\left\{\widehat{\boldsymbol{Q}'}_{r,d}\right\}$.

Now observe that the criterion in (52) is a *quartic* function with respect to $\boldsymbol{s}$, which is in fact difficult to minimize. However, similar to the proposed transition from (30) to (31), we can derive a *quadratic* alternative to (52): for any generic positive-definite matrix $\boldsymbol{Q}$, the quantity $\boldsymbol{s}^H \boldsymbol{Q} \boldsymbol{s}$ is *close* to λN if and only if the l_2-norm of $\boldsymbol{R}\boldsymbol{s}$ is *close* to $\sqrt{\lambda N}$, where $\boldsymbol{R}$ denotes the Hermitian square root of $\boldsymbol{Q}$, i.e. $\boldsymbol{Q} = \boldsymbol{R}^H \boldsymbol{R}$. Equivalently, $\boldsymbol{s}^H \boldsymbol{Q} \boldsymbol{s}$ is *close* to λN if and only if there exists a unit-norm vector $\boldsymbol{u}$ such that $\boldsymbol{R}\boldsymbol{s}$ is *close* to $\sqrt{\lambda N}\boldsymbol{u}$. As a result, (52) can be made *small* conveniently by tackling the following alternative quadratic optimization problem [21]–[24]:

$$\begin{aligned} \min_{\boldsymbol{s},\{\widetilde{\boldsymbol{u}}_{r,d}\},\{\widehat{\boldsymbol{u}}_{r,d}\}} \quad & \overline{\zeta} \\ \text{s.t.} \quad & |\boldsymbol{s}_n| \quad = 1, \quad n = 1, \ldots, N, \\ & \|\widetilde{\boldsymbol{u}}_{r,d}\|_2 = \|\widehat{\boldsymbol{u}}_{r,d}\|_2 = 1, \end{aligned} \tag{54}$$

where

$$\begin{aligned} \overline{\zeta} = \sum_{r=0}^{N_r-1} \sum_{\substack{d=-(N_d-1) \\ (r,d)\neq(0,0)}}^{N_d-1} & \left\{ \left\|\widetilde{\boldsymbol{R}}_{r,d} \boldsymbol{s} - \sqrt{\lambda N}\widetilde{\boldsymbol{u}}_{r,d}\right\|^2 \right. \\ & \left. + \left\|\widehat{\boldsymbol{R}}_{r,d} \boldsymbol{s} - \sqrt{\lambda N}\widehat{\boldsymbol{u}}_{r,d}\right\|^2 \right\}, \end{aligned} \tag{55}$$

and $\widetilde{\boldsymbol{R}}_{r,d}$, $\widehat{\boldsymbol{R}}_{r,d}$ are the Hermitian square roots of $\widetilde{\boldsymbol{Q}'}_{r,d}$, $\widehat{\boldsymbol{Q}'}_{r,d}$, respectively, i.e. $\widetilde{\boldsymbol{Q}'}_{r,d} = \widetilde{\boldsymbol{R}}_{r,d}^H \widetilde{\boldsymbol{R}}_{r,d}$, $\widehat{\boldsymbol{Q}'}_{r,d} = \widehat{\boldsymbol{R}}_{r,d}^H \widehat{\boldsymbol{R}}_{r,d}$. To tackle the minimization problem in (54), we adopt a cyclic method as follows. For given $\boldsymbol{s}$, the minimization of (54) with

respect to $\{\widetilde{\boldsymbol{u}}_{r,d}\}$ and $\{\widehat{\boldsymbol{u}}_{r,d}\}$ is immediate:

$$\widetilde{\boldsymbol{u}}_{r,d} = \frac{\widetilde{\boldsymbol{R}}_{r,d}\boldsymbol{s}}{\|\widetilde{\boldsymbol{R}}_{r,d}\boldsymbol{s}\|_2}, \tag{56}$$

$$\widehat{\boldsymbol{u}}_{r,d} = \frac{\widehat{\boldsymbol{R}}_{r,d}\boldsymbol{s}}{\|\widehat{\boldsymbol{R}}_{r,d}\boldsymbol{s}\|_2}. \tag{57}$$

Next, for given $\{\widetilde{\boldsymbol{u}}_{r,d}\}$ and $\{\widehat{\boldsymbol{u}}_{r,d}\}$, the objective of (54) can be reformulated as

$$\begin{aligned}
\overline{\zeta} &= \sum_{r=0}^{N_r-1} \sum_{\substack{d=-(N_d-1)\\(r,d)\neq(0,0)}}^{N_d-1} \Big\{ \left\| \widetilde{\boldsymbol{R}}_{r,d}\boldsymbol{s} - \sqrt{\lambda N}\widetilde{\boldsymbol{u}}_{r,d} \right\|^2 \\
&\qquad + \left\| \widehat{\boldsymbol{R}}_{r,d}\boldsymbol{s} - \sqrt{\lambda N}\widehat{\boldsymbol{u}}_{r,d} \right\|^2 \Big\} \\
&= \sum_{r=0}^{N_r-1} \sum_{\substack{d=-(N_d-1)\\(r,d)\neq(0,0)}}^{N_d-1} \Big\{ \boldsymbol{s}^H \left(\widetilde{\boldsymbol{R}}_{r,d}^H \widetilde{\boldsymbol{R}}_{r,d} + \widehat{\boldsymbol{R}}_{r,d}^H \widehat{\boldsymbol{R}}_{r,d} \right) \boldsymbol{s} \\
&\qquad - 2\sqrt{\lambda N}\, \Re\left\{ \boldsymbol{s}^H \left(\widetilde{\boldsymbol{R}}_{r,d}^H \widetilde{\boldsymbol{u}}_{r,d} + \widehat{\boldsymbol{R}}_{r,d}^H \widehat{\boldsymbol{u}}_{r,d} \right) \right\} \Big\} + \text{const.} \\
&= \boldsymbol{s}^H \boldsymbol{R} \boldsymbol{s} + 2\,\Re\{\boldsymbol{s}^H \boldsymbol{u}\} + \text{const.}
\end{aligned} \tag{58}$$

where

$$\begin{aligned}
\boldsymbol{R} &= \sum_{r=0}^{N_r-1} \sum_{\substack{d=-(N_d-1)\\(r,d)\neq(0,0)}}^{N_d-1} \left(\widetilde{\boldsymbol{R}}_{r,d}^H \widetilde{\boldsymbol{R}}_{r,d} + \widehat{\boldsymbol{R}}_{r,d}^H \widehat{\boldsymbol{R}}_{r,d} \right) \\
&= \sum_{r=0}^{N_r-1} \sum_{\substack{d=-(N_d-1)\\(r,d)\neq(0,0)}}^{N_d-1} \left(\widetilde{\boldsymbol{Q}'}_{r,d} + \widehat{\boldsymbol{Q}'}_{r,d} \right),
\end{aligned} \tag{59}$$

$$\boldsymbol{u} = -\sqrt{\lambda N} \sum_{r=0}^{N_r-1} \sum_{\substack{d=-(N_d-1)\\(r,d)\neq(0,0)}}^{N_d-1} \left(\widetilde{\boldsymbol{R}}_{r,d}^H \widetilde{\boldsymbol{u}}_{r,d} + \widehat{\boldsymbol{R}}_{r,d}^H \widehat{\boldsymbol{u}}_{r,d} \right).$$

Now by dropping the constant part in (58), we obtain the following objective function:

$$\begin{aligned}
&\boldsymbol{s}^H \boldsymbol{R} \boldsymbol{s} + 2\Re(\boldsymbol{s}^H \boldsymbol{u}) \\
&= \begin{pmatrix} \boldsymbol{s} \\ 1 \end{pmatrix}^H \begin{pmatrix} \boldsymbol{R} & \boldsymbol{u} \\ \boldsymbol{u}^H & 0 \end{pmatrix} \begin{pmatrix} \boldsymbol{s} \\ 1 \end{pmatrix} \\
&= \tilde{\boldsymbol{s}}^H \boldsymbol{C} \tilde{\boldsymbol{s}}
\end{aligned} \tag{60}$$

Therefore, the minimization of (54) with respect to $\boldsymbol{s}$ is equivalent to

$$\begin{aligned}
\min_{\boldsymbol{s}} \quad & \tilde{\boldsymbol{s}}^H \boldsymbol{C} \tilde{\boldsymbol{s}} \\
\text{s.t.} \quad & |\boldsymbol{s}_n| = 1,\ n = 1, \ldots, N; \\
& \tilde{\boldsymbol{s}} = \begin{pmatrix} \boldsymbol{s} \\ 1 \end{pmatrix}.
\end{aligned} \tag{61}$$

As a result of the unimodular constraint, $\tilde{\boldsymbol{s}}$ has a fixed l_2-norm, and hence, a diagonal loading of $\boldsymbol{C}$ does not change the solution to (61). Thus, (61) can be written in the following equivalent form:

$$\begin{aligned}
\max_{\boldsymbol{s}} \quad & \tilde{\boldsymbol{s}}^H \widetilde{\boldsymbol{C}} \tilde{\boldsymbol{s}} \\
\text{s.t.} \quad & |\boldsymbol{s}_n| = 1,\ n = 1, \ldots, N; \\
& \tilde{\boldsymbol{s}} = \begin{pmatrix} \boldsymbol{s} \\ 1 \end{pmatrix};
\end{aligned} \tag{62}$$

where $\widetilde{\boldsymbol{C}} = \lambda' \boldsymbol{I} - \boldsymbol{C}$, with λ' being larger than the maximum eigenvalue of $\boldsymbol{C}$. The maximization problem (62) is in fact a UQP [25], and can be tackled efficiently by the power method-like iterations originally proposed in [25], [26], viz.

$$\boldsymbol{s}^{(t+1)} = \exp\left\{ j \arg\left(\begin{pmatrix} \boldsymbol{I}_{N\times N} \\ \boldsymbol{0}_{1\times N} \end{pmatrix}^T \widetilde{\boldsymbol{C}} \tilde{\boldsymbol{s}}^{(t)} \right) \right\} \tag{63}$$

where the iterations can be initialized with the latest design of $\boldsymbol{s}$ (used as $\boldsymbol{s}^{(0)}$) and t denotes the internal iteration number. Finally, the steps of the proposed algorithm for designing the transmit signal $\boldsymbol{s}$ is summarized in Table III. As to the computational cost, the suggested algorithm relies on a one-time computation of the matrices matrices $\widetilde{\boldsymbol{Q}}_{r,d}$ and $\widehat{\boldsymbol{Q}}_{r,d}$ and their Cholesky decomposition with an $\mathcal{O}(N_r N_d (L + N^2 + N^3))$ cost. Then, at each iteration, the proposed method requires simple matrix multiplications with $\mathcal{O}(N^2\eta)$ cost where η denotes the number of employed power method-like iterations.

TABLE III
THE ALGORITHM FOR SPARSITY-AWARE TRANSMIT SEQUENCE DESIGN (PULSE-TRAIN CASE)

Step 0: Set the $\boldsymbol{s}$ to some initial values (e.g., $\boldsymbol{s}$ can be randomly generated or given by a good existing sequence) and calculate the matrices $\widetilde{\boldsymbol{Q}}_{r,d}$ and $\widehat{\boldsymbol{Q}}_{r,d}$. using (48) and (49).
Step 1: Compute $\widetilde{\boldsymbol{u}}_{r,d}$ and $\widehat{\boldsymbol{u}}_{r,d}$ using (56) and (57) for $\boldsymbol{s}$ fixed.
Step 2: Use the power method-like iterations in (63) (until convergence) to obtain $\boldsymbol{s}$.
Step 3: Repeat steps 1 and 2 until a stop criterion is satisfied, e.g. $\|\boldsymbol{s}^{(i+1)} - \boldsymbol{s}^{(i)}\|_F < \varepsilon$ for some given $\varepsilon > 0$, where i denotes the total iteration number.

Remark on Optimality: The optimization problems emerging from coherence reduction scenarios are often multimodal (i.e. they have many local optima); see e.g. [22], [27]–[30]. Given the non-convex nature of the design, one usually settles for approximation algorithms with the goal of finding the local optima of the problem. However, it is interesting to note that similar formulations to ones in this paper have been successful in approaching the fundamental limits of coherence (such as the Welch bounds on peak and integrated coherence level) [31]–[33]—which presumably is due to the commonly observed property that the optimization landscape in coherence reduction may, in fact, contain many global optima, or many local optima whose coherence is pretty close to the global optimum from a practical viewpoint [31], [34]. ■

VI. SIMULATION RESULTS

Hereafter, we investigate the performance of the proposed approaches in comparison to well-established alternative transmit waveforms available in the literature. We consider employing the proposed methods to design a transmit sequence $\boldsymbol{s}$ of

length $N = 127$, using the Alltop sequence as initialization, for a target scene with $N_r = 20$ range and $N_d = 15$ Doppler bins. The Alltop sequence is known to yield a good incoherence property of the sensing matrix $\mathbf{\Phi}$ [15], and is defined for prime lengths $N > 5$ as

$$\boldsymbol{s}_{Alltop}(n) = e^{j\frac{2\pi}{N}n^3}, \quad n = 1, 2, \ldots, N. \tag{64}$$

In addition to the Alltop sequence, we also use the random phase sequence ($e^{j\theta_n}, \{\theta_n\}$ are independent random variables uniformly distributed in $[0, 2\pi]$) and the m-sequence [35], [36] for comparison. The root mean-square error (RMSE) of target scene recovery, i.e. the recovery of $\boldsymbol{\alpha}$, is defined as $\|\tilde{\boldsymbol{\alpha}} - \boldsymbol{\alpha}\|_2$ where $\tilde{\boldsymbol{\alpha}}$ denotes the recovered target scene. We stop the optimization algorithms whenever the l_2-norm of change in the designed signal becomes smaller than $\varepsilon = 10^{-3}$.

A. Single-pulse

1) Incoherence: We first compare the coherence coefficients in single-pulse scenario associated with the random phase sequence, m-sequence, Alltop sequence and the optimized sequence obtained by the proposed method. The results are shown in Fig. 2. It can be observed from Fig. 2 that although the maximum coherence values for all the sequences are the same, the coherence values corresponding to the optimized sequence are in general considerably lower than the other three sequences considered in this example.

2) Target Scene Recovery: In order to verify the effectiveness of the optimized sequences, we examine the success rate and RMSE of the target scene recovery for different signal-to-noise ratio (SNR) values. We construct the sparse vectors $\boldsymbol{\alpha}$ by choosing $K = 30$ non-zero locations in the vector, with identical chance for all $\binom{N_d N_r}{K}$ assignments of the non-zero locations, and consider random positive RCS values for the non-zero locations. We use OMP as the recovery algorithm and consider a target scene recovery successful if and only if all the non-zero locations of the estimated sparse vector $\tilde{\boldsymbol{\alpha}}$ are the same as those of the true targets scene $\boldsymbol{\alpha}$. Fig. 3 presents the recovery results. In this case, it is interesting to observe that, except for the optimized sequence, the other three sequences can not recover all of the target scenes correctly even for large SNR values (the success rate is less than one).

It can be also interesting to see how the sparsity order $K = \|\boldsymbol{\alpha}\|_0$ affects the recovery performance. To this end, Fig. 4 shows the recovery success rates and RMSEs for different sparsity orders K of the target scene with SNR$=$ 0dB. The results leading to Fig. 3 and Fig. 4 are obtained by averaging over the simulation results from 500 Monte Carlo experiments (with different random initializations).

B. Pulse-train

1) Incoherence: Similar to the previous case, we compare the coherence coefficients of random phase sequence, m-sequence, Alltop sequence and the optimized sequence obtained by the proposed method in pulse-train scenario. We set the number of active pulses to $L = 10$. The results are shown in Fig. 5. It can be observed from Fig. 5 that the optimized sequence outperforms the other three sequences in terms of incoherence. It is interesting to note that, in light of the recovery condition in (13), a smaller mutual coherence associated with the optimized sequence guarantees the ability of the radar system to recover target scenes with larger number of targets (i.e. with larger K).

We further note that, compared to Fig. 2, the coherence coefficients associated with all sequences in the pulse-train scenario are considerably smaller than those in the single-pulse case. Such an expected outcome leads to better recovery results in the pulse-train scenario; see below.

2) Target Scene Recovery: As shown in Fig. 5, the sequences working in pulse-train scenario have good coherence features. Thus, as discussed earlier, the sequence can be applied to more severe situations (specially with low SNR or large sparsity order K). Fig. 6 demonstrates the recovery results for different SNR values, with $L = 10$ and $K = 90$. According to Fig. 6, satisfactory recovery results can be achieved even for low SNR and large sparsity order conditions by employing the sequence obtained by the proposed method. The results leading to Fig. 6 are obtained by averaging the simulation results for 500 Monte Carlo experiments (with different random initializations). Similar to the previous case, OMP is employed as the recovery algorithm.

VII. Conclusion

We presented a modeling of the radar system and particularly the transmit waveforms in the sparsity-aware scenarios. Depending on the structure of transmit waveforms, namely the single-pulse and pulse-train cases, efficient waveform optimization algorithms were proposed for a judicious design of the radar signals. It was shown that optimizing the radar transmit waveforms leads to smaller coherence coefficients and better recovery results than not only random sequences but also other sequences known for their good measurement properties. Note that, although pulse-train waveforms are longer and more costly for transmission than their single-pulse counterparts, they usually lead to better target scence recovery. Interestingly, for the CS-based radar system, it was confirmed from the simulation results that using pulse-train signals is advantageous in terms of recovery performance—a coherent observation with that typically made in traditional radar systems.

References

[1] H. Hu, M. Soltanalian, P. Stoica, and X. Zhu, "Sparsity-aided radar waveform synthesis," in *22nd European Signal Processing Conference (EUSIPCO)*, Lisbon, Portugal, 2014, pp. 2270–2274.

[2] D. Donoho, "Compressed sensing," *IEEE Transactions on Information Theory*, vol. 52, no. 4, pp. 1289–1306, April 2006.

[3] E. Candès and M. Wakin, "An introduction to compressive sampling," *IEEE Signal Processing Magazine*, vol. 25, no. 2, pp. 21–30, March 2008.

[4] Y. He, X. Zhu, S. Zhuang, H. Li, and H. Hu, "Waveform optimization for compressive sensing radar imaging," in *IEEE CIE International Conference on Radar*, vol. 2. Chengdu, China: IEEE, 2011, pp. 1263–1266.

[5] R. Baraniuk and P. Steeghs, "Compressive radar imaging," in *IEEE Radar Conference*. IEEE, 2007, pp. 128–133.

[6] M. Herman and T. Strohmer, "Compressed sensing radar," in *IEEE Radar Conference*. IEEE, 2008, pp. 1–6.

[7] Y. Yu, A. P. Petropulu, and H. V. Poor, "MIMO radar using compressive sampling," *IEEE Journal of Selected Topics in Signal Processing*, vol. 4, no. 1, pp. 146–163, 2010.

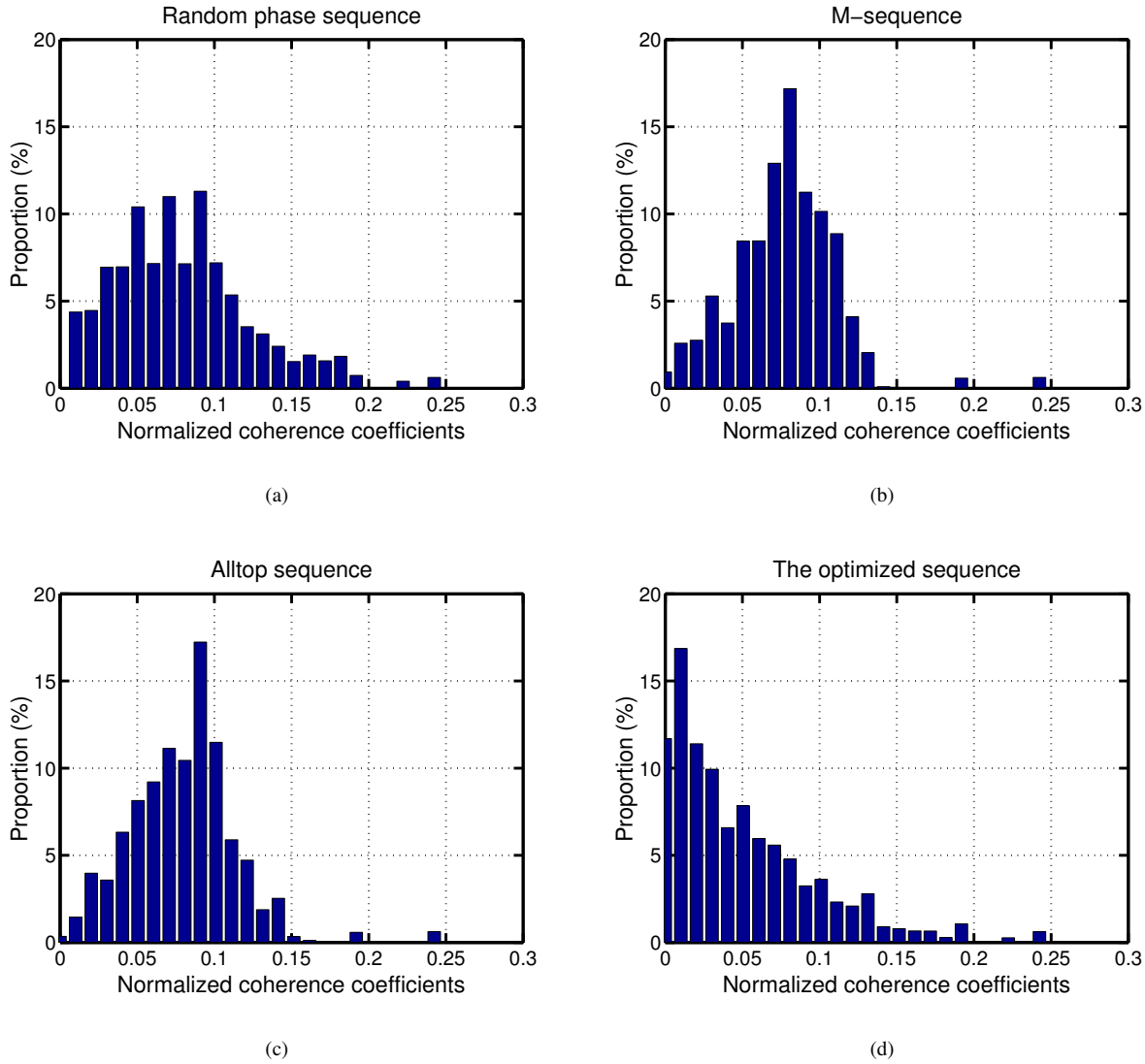

Fig. 2. Distribution of the coherence coefficients in single-pulse scenario; associated with (a) random phase sequence, (b) m-sequence, (c) Alltop sequence, and (d) the optimized sequence obtained by the proposed method (using the Alltop sequence as initialization).

[8] W. Roberts, T. Yardibi, J. Li, X. Tan, and P. Stoica, "Sparse signal representation for MIMO radar imaging," in *42nd Asilomar Conference on Signals, Systems and Computers*. CA, USA: IEEE, 2008, pp. 609–613.

[9] V. M. Patel, G. R. Easley, D. M. Healy Jr, and R. Chellappa, "Compressed synthetic aperture radar," *IEEE Journal of Selected Topics in Signal Processing*, vol. 4, no. 2, pp. 244–254, 2010.

[10] L. Zhang, M. Xing, C.-W. Qiu, J. Li, J. Sheng, Y. Li, and Z. Bao, "Resolution enhancement for inversed synthetic aperture radar imaging under low SNR via improved compressive sensing," *IEEE Transactions on Geoscience and Remote Sensing*, vol. 48, no. 10, pp. 3824–3838, October 2010.

[11] J. Zhang, D. Zhu, and G. Zhang, "Adaptive compressed sensing radar oriented toward cognitive detection in dynamic sparse target scene," *IEEE Transactions on Signal Processing*, vol. 60, no. 4, pp. 1718–1729, April 2012.

[12] L. C. Potter, E. Ertin, J. T. Parker, and M. Cetin, "Sparsity and compressed sensing in radar imaging," *Proceedings of the IEEE*, vol. 98, no. 6, pp. 1006–1020, 2010.

[13] N. S. Subotic, B. Thelen, K. Cooper, W. Buller, J. Parker, J. Browning, and H. Beyer, "Distributed radar waveform design based on compressive sensing considerations," in *IEEE Radar Conference*. IEEE, 2008, pp. 1–6.

[14] H. He, J. Li, and P. Stoica, *Waveform design for active sensing systems: a computational approach*. Cambridge University Press, 2012.

[15] M. Herman and T. Strohmer, "High-resolution radar via compressed sensing," *IEEE Transactions on Signal Processing*, vol. 57, no. 6, pp. 2275–2284, June 2009.

[16] M. Skolnik, *Introduction to Radar Systems*. Tata McGraw Hill, 2003.

[17] O. Bar-Ilan and Y. Eldar, "Sub-Nyquist radar via Doppler focusing," *IEEE Transactions on Signal Processing*, vol. 62, no. 7, pp. 1796–1811, April 2014.

[18] E. J. Candès, J. K. Romberg, and T. Tao, "Stable signal recovery from incomplete and inaccurate measurements," *Communications on pure and applied mathematics*, vol. 59, no. 8, pp. 1207–1223, 2006.

[19] R. Baraniuk, "Compressive sensing," *IEEE signal processing magazine*, vol. 24, no. 4, 2007.

[20] M. Elad, *Sparse and redundant representations: from theory to applications in signal and image processing*. New York, NY: Springer, 2010.

[21] H. He, P. Stoica, and J. Li, "Designing unimodular sequence sets with good correlations—including an application to MIMO radar," *IEEE Transactions on Signal Processing*, vol. 57, no. 11, pp. 4391–4405, 2009.

[22] J. A. Tropp, I. S. Dhillon, R. W. Heath, and T. Strohmer, "Designing structured tight frames via an alternating projection method," *IEEE Transactions on Information Theory*, vol. 51, no. 1, pp. 188–209, 2005.

[23] J. Li, P. Stoica, and X. Zheng, "Signal synthesis and receiver design for MIMO radar imaging," *IEEE Transactions on Signal Processing*, vol. 56, no. 8, pp. 3959–3968, 2008.

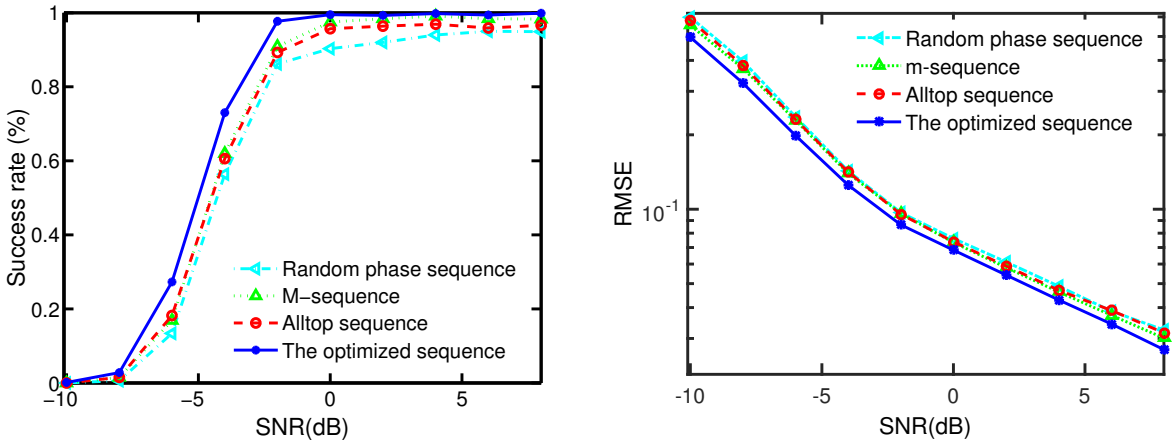

(a) (b)

Fig. 3. The recovery results in single-pulse scenario for different values of SNR (with number of targets $K = 30$): (a) success rate, (b) RMSE.

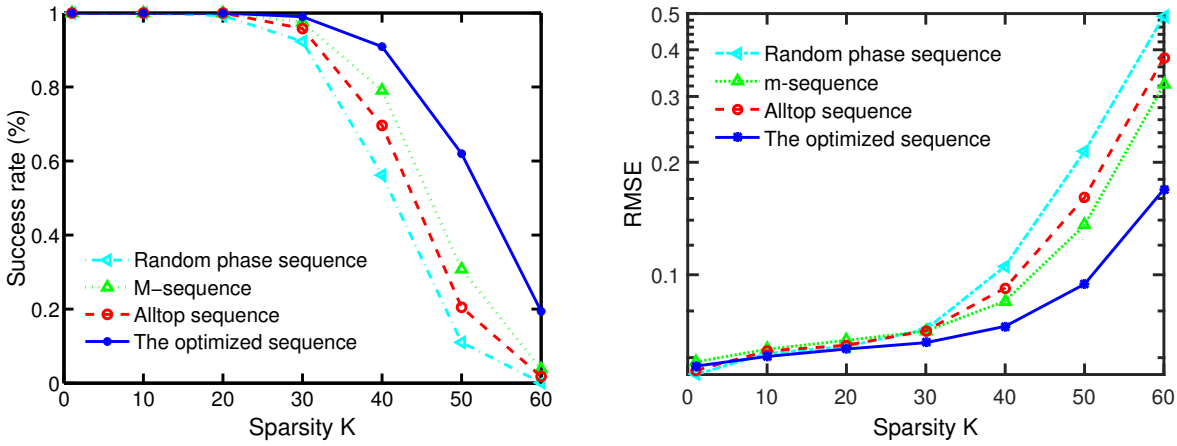

(a) (b)

Fig. 4. The recovery results in single-pulse scenario for different sparsity orders K of the target scene α: (a) success rate, (b) RMSE.

[24] M. Soltanalian, H. Hu, and P. Stoica, "Single-stage transmit beamforming design for MIMO radar," *Signal Processing*, vol. 102, pp. 132–138, 2014.

[25] M. Soltanalian and P. Stoica, "Designing unimodular codes via quadratic optimization," *IEEE Transactions on Signal Processing*, vol. 62, no. 5, pp. 1221–1234, 2014.

[26] M. Soltanalian, B. Tang, J. Li, and P. Stoica, "Joint design of the receive filter and transmit sequence for active sensing." *IEEE Signal Process. Lett.*, vol. 20, no. 5, pp. 423–426, 2013.

[27] P. Stoica, H. He, and J. Li, "New algorithms for designing unimodular sequences with good correlation properties," *IEEE Transactions on Signal Processing*, vol. 57, no. 4, pp. 1415–1425, 2009.

[28] M. Soltanalian, M. M. Naghsh, and P. Stoica, "On meeting the peak correlation bounds," *IEEE Transactions on Signal Processing*, vol. 62, no. 5, pp. 1210–1220, March 2014.

[29] M. Soltanalian and P. Stoica, "Computational design of sequences with good correlation properties," *IEEE Transactions on Signal Processing*, vol. 60, no. 5, pp. 2180–2193, 2012.

[30] P. Stoica, H. He, and J. Li, "On designing sequences with impulse-like periodic correlation," *IEEE Signal Processing Letters*, vol. 16, no. 8, pp. 703–706, 2009.

[31] H. He, P. Stoica, and J. Li, "On aperiodic-correlation bounds," *IEEE Signal Processing Letters*, vol. 17, no. 3, pp. 253–256, 2010.

[32] L. R. Welch, "Lower bounds on the maximum cross correlation of signals (corresp.)," *IEEE Transactions on Information Theory*, vol. 20, no. 3, pp. 397–399, 1974.

[33] D. V. Sarwate, "Meeting the Welch bound with equality," in *Sequences and their Applications*. Springer, 1999, pp. 79–102.

[34] J. J. Benedetto, I. Konstantinidis, and M. Rangaswamy, "Phase-coded waveforms and their design," *IEEE Signal Processing Magazine*, vol. 26, no. 1, pp. 22–31, 2009.

[35] T. Soderstrom and P. Stoica, *System Identification*. Prentice Hall London, 1989.

[36] N. Levanon and E. Mozeson, *Radar Signals*. John Wiley & Sons, 2004.

[37] Y.-S. Yoon and M. G. Amin, "Compressed sensing technique for high-resolution radar imaging," in *SPIE Defense and Security Symposium*. International Society for Optics and Photonics, 2008, pp. 69 681A–69 681A.

[38] M. G. Amin, *Compressive sensing for urban radar*. CRC Press, 2014.

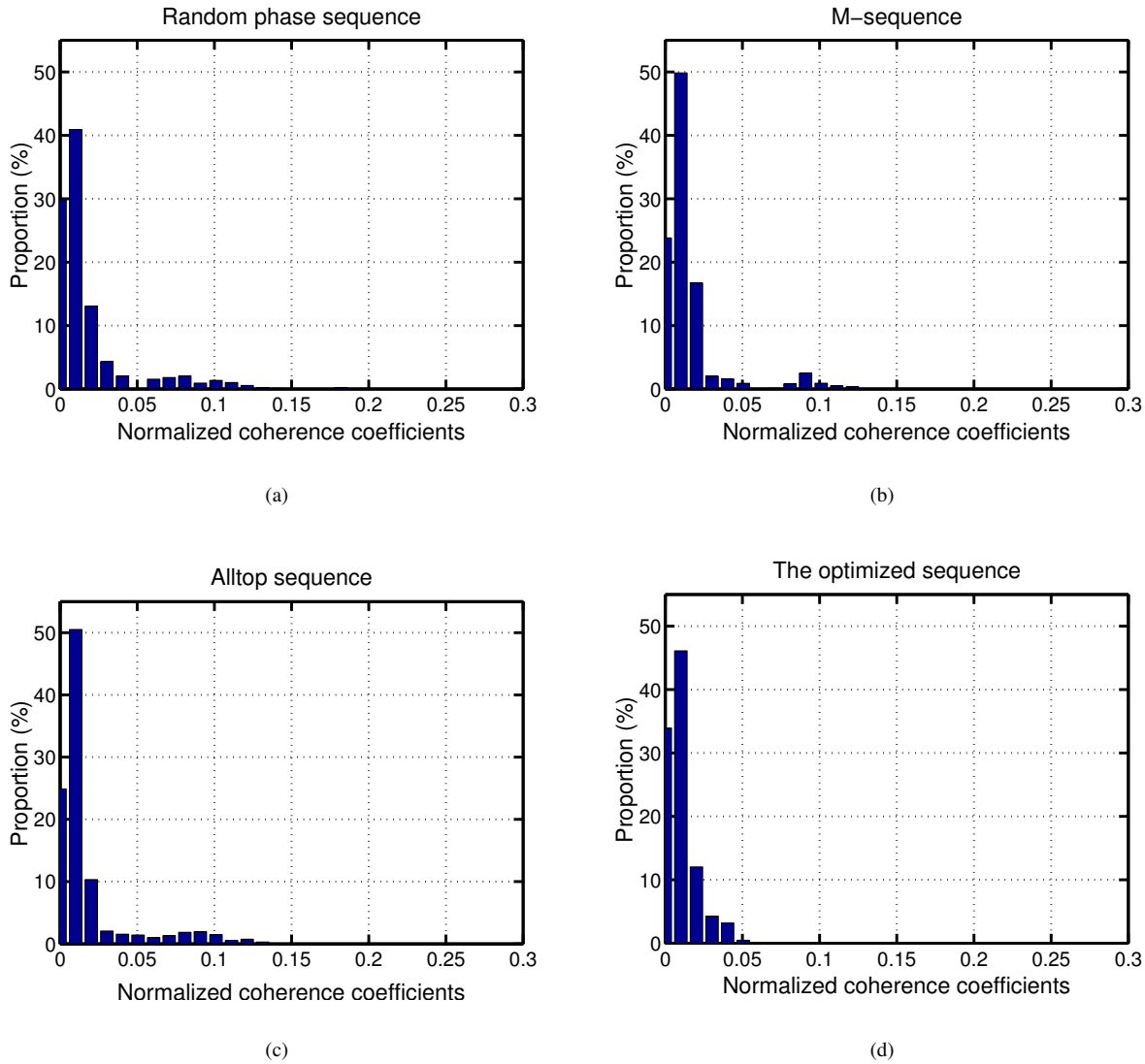

(a) (b) (c) (d)

Fig. 5. Distribution of the coherence coefficients in pulse-train scenario; associated with (a) random phase sequence, (b) m-sequence, (c) Alltop sequence and (d) the optimized sequence obtained by the proposed method using the Alltop sequence as initialization, respectively.

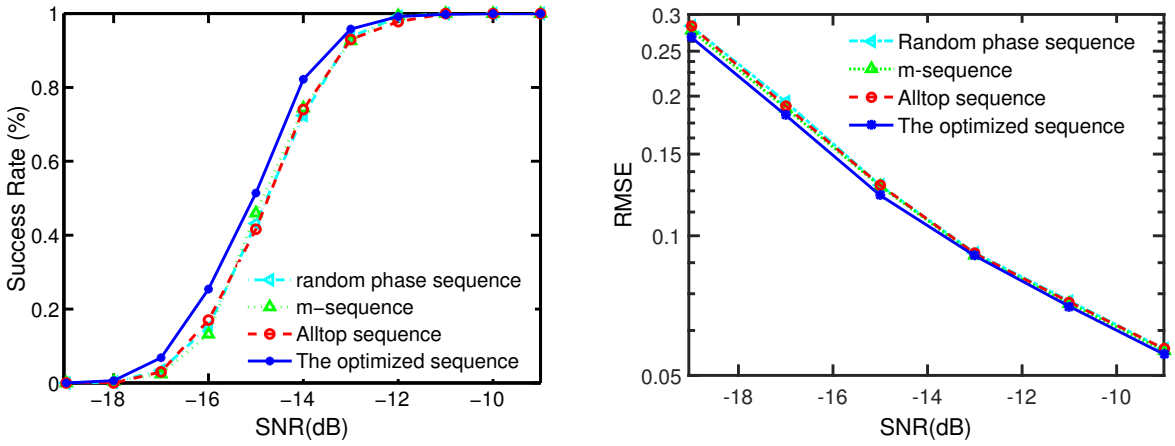

(a) (b)

Fig. 6. The recovery results in pulse-train scenario for different values of SNR: (a) success rate, (b) RMSE.